Linear Parameter Varying Controller Design For Satellite Attitude Control ⋆

Emily Burgin * **Felix Biertümpfel** * **Harald Pfifer** *

* *Chair of Flight Mechanics and Control, Technische Universität Dresden, Dresden, 01062 Germany (e-mail: {emily.burgin, felix.biertuempfel, harald.pfifer}@tu-dresden.de).*

Abstract: This paper presents a systematic linear parameter varying (LPV) control approach for the 3-axis attitude control of an Earth-observation satellite in a sun-synchronous orbit. The dynamics of the satellite depend on the orientation of the solar array, which completes a full rotation every orbit, thus it is used as a scheduling parameter in the design. The satellite has two additional flexible appendages; these are 2 scatterometers. The control objective is to precisely track a given reference attitude using reaction wheels, while rejecting external torque disturbances and sensor noise. The design follows a mixed-sensitivity approach, applying a recently introduced weighting scheme. It allows traceable and effective controller tuning by using a low number of physically interpretable weights. The controller is synthesised by solving the induced L_2-norm of the closed-loop interconnection of the controller and weighted plant. Scheduling with the solar array orientation leads to an LPV notching behaviour in the controller that effectively mitigates the effects of the array's most prominent flexible modes. This behaviour enables increased performance, when compared to a linear time invariant controller, while maintaining robustness. The pointing performance of the synthesised controller over the complete satellite lifecycle is verified using the European Space Agency's standards for spacecraft attitude control.

Keywords: Linear parameter-varying systems, robust control, aerospace, disturbance rejection, tracking, high accuracy pointing

1. INTRODUCTION

Observation satellites must fulfil stringent pointing requirements in order to produce high quality image data. For this purpose, they are equipped with attitude control systems. These control systems must operate accurately under varying system dynamics as well as complex environmental disturbances. To achieve optimal performance at all times, the controller must be able to adapt to changes in the spacecraft dynamics. Some of these changes result from measurable parameter variations, which can then be explicitly considered in the design and used for controller scheduling during operations. Moreover, the resulting controller must be robust towards uncertainty in the system dynamics over the satellite's life cycle. Given that satellite pointing performance requirements are frequency-based, H_∞ control is the logical framework to directly incorporate the requirements into the design. A linear parameter varying (LPV) framework that uses insights from classical H_∞ then provides an efficient approach to address both robustness and varying system dynamics effectively. It is able to provide an optimal robust controller scheduled with the measurable parameters in a single synthesis. Additionally, design and analysis of LPV controllers can be conducted using readily available tools such as the LPVTools toolbox in MATLAB (Hjartarson et al., 2015).

⋆ This work is partially supported by ESA Project No. AO/1-11017/21/NL/MGu entitled *Adaptable Control and Estimation with Guaranteed Robust Performance.*

Fig. 1. MetOp-SG Satellite (ESA, 2013).

In recent years, there is growing interest in modelling dynamical systems with respect to variable parameters, as in Kassarian et al. (2022). Within the aerospace industry, there are tools available for the modelling of uncertain flexible space structures (Alazard and Sanfedino, 2020) and methods for controlling them (Angeletti et al., 2022). There are also techniques for obtaining linear models of spacecraft that are parameterised with the motion of flexible appendages, as in Guy et al. (2014). By extension, the present paper details an LPV approach for the reaction wheel based attitude control of an industry-standard Earth-observation satellite that is parameterised with the motion of a flexible solar array.

The given satellite has a flexible solar array that rotates 360°, with a fixed angular rate, every orbit. It also has two additional flexible appendages and uncertain mass and dimensional properties. Eumetsat's MetOp and MetOp-SG satellites are typical examples of such spacecraft, pictured in Fig. 1. The biggest driver in the proposed design is the rotating solar array, which changes the dynamics of the spacecraft throughout the mission. Because of this, the LPV design is scheduled with the motion of the array in a grid-based approach, which is particularly suited to the proposed problem due to the slow nature of the parameter variation and resulting dynamical changes.

It is also important to consider that, in an industrial setting, the design process must be well established, versatile for different use-cases and intuitive for the design engineer to follow. To address these matters, the control design applies a recently proposed weighting scheme (Theis et al., 2020) to the grid-based LPV controller synthesis. It facilitates highly traceable and particularly easy tuning as the system requirements and constraints directly translate into the weights. The scheme's versatility has so far been demonstrated on launchers (Biertümpfel et al., 2022), flexible aircraft (Theis et al., 2020) and auto-landing problems (Theis et al., 2018). Applying this mixed-sensitivity weighting scheme using the grid-based LPV method is motivated by a combination of optimal robust control for flexible systems and traditional aircraft gain-scheduling control design. It has the advantages of H_∞ controller design with the additional benefit that the synthesised controller is automatically scheduled.

2. LINEAR PARAMETER VARYING SYSTEMS

LPV systems are a class of systems whose state space matrices depend continuously on a time-varying parameter vector $\rho : \mathbb{R} \to \mathcal{P}$, where $\mathcal{P} \in \mathbb{R}^{n_\rho}$ is a compact subset chosen based on physical considerations. In addition, the parameter rates of variation $\dot{\rho}$ are assumed to lie within a hyper-rectangle $\dot{\mathcal{P}}$ defined by $\dot{\mathcal{P}} = \{\dot{\rho}(t) \in \mathbb{R}^{n_\rho} | \, |\rho_i(t)| \leq \nu_i, i = 1, \ldots, n_\rho\}$. Hence, the set of all admissible trajectories is $\mathcal{T} = \{\rho : \mathbb{R} \to \mathcal{P} | \, \rho \in \mathcal{C}^1, \rho(t) \in \mathcal{P} \text{ and } \dot{\rho}(t) \in \dot{\mathcal{P}} \, \forall t \geq 0\}$.

The state space matrices of an LPV system are continuous functions of the parameter vector, i.e., $A : \mathcal{P} \to \mathbb{R}^{n_x \times n_x}$, $B : \mathcal{P} \to \mathbb{R}^{n_x \times n_u}$, $C : \mathcal{P} \to \mathbb{R}^{n_y \times n_x}$, and $D : \mathcal{P} \to \mathbb{R}^{n_y \times n_u}$. An n_x^{th}-order LPV system G_ρ is defined by

$$\begin{bmatrix} \dot{x}(t) \\ y(t) \end{bmatrix} = \begin{bmatrix} A(\rho(t)) & B(\rho(t)) \\ C(\rho(t)) & D(\rho(t)) \end{bmatrix} \begin{bmatrix} x(t) \\ u(t) \end{bmatrix}, \tag{1}$$

where $x(t) \in R_x^n$ is the state, $u(t) \in R_u^n$ the input, and $y(t) \in R_y^n$ the output. The explicit dependence on t is occasionally omitted to shorten the notation.

2.1 Induced L_2-norm controller synthesis

The performance of an LPV system can be specified in terms of its induced L_2-norm

$$\|G_\rho\| = \sup_{u \in \mathbb{L}_2 \setminus \{0\}, \rho \in \mathcal{T}, x(0)=0} \frac{\|y\|_2}{\|u\|_2}. \tag{2}$$

A generalization of the Bounded Real Lemma (Wu et al., 1996) provides a sufficient condition to upper bound $\|G_\rho\|$. The next theorem states this condition.

Theorem 1. (Wu et al., 1996): G_ρ is exponentially stable and $\|G_\rho\| \leq \gamma$ if there exists a continuously differentiable symmetric matrix function $P : \mathcal{P} \to \mathbb{R}^{n_x \times n_x}$ such that $P(p) \geq 0$ and

$$\begin{bmatrix} PA + A^T P + \partial P & PB \\ B^T P & -I \end{bmatrix} + \frac{1}{\gamma^2} \begin{bmatrix} C^T \\ D^T \end{bmatrix} \begin{bmatrix} C & D \end{bmatrix} \leq 0 \tag{3}$$

hold for all $p \in \mathcal{P}$ and $q \in \dot{\mathcal{P}}$, where ∂P is defined as $\partial P(p, q) = \sum_{i=1}^{n_\rho} \frac{\partial P}{\partial \rho_i}(p) q_i$. In (3), the dependence of the matrices on p and q has been omitted to shorten the notation.

This theorem forms the basis for the induced L_2-norm controller synthesis in Wu et al. (1996). In short, consider an open loop LPV system G_ρ with inputs $[w^T, u^T]^T$ and outputs $[z^T, y^T]^T$. The objective is to synthesize a controller K_ρ:

$$\begin{bmatrix} \dot{x}_K \\ u \end{bmatrix} = \begin{bmatrix} A_K(\rho) & B_K(\rho) \\ C_K(\rho) & D_K(\rho) \end{bmatrix} \begin{bmatrix} x_K \\ y \end{bmatrix} \tag{4}$$

such that the induced L_2-gain of the closed loop interconnection of G_ρ and K_ρ, denoted by the lower fractional transformation $F_l(G_\rho, K_\rho)$, is minimized

$$\min_{K_\rho} \|F_l(G_\rho, K_\rho)\| \tag{5}$$

This optimization problem can be solved via parametrized LMI conditions, see Wu et al. (1996) for details. It should be noted that the synthesis problem involves an infinite collection of LMI constraints parametrized by $(p, q) \in \mathcal{P} \times \dot{\mathcal{P}}$. A remedy to this issue, which works in many practical examples, is to approximate them with finite-dimensional LMIs evaluated on a grid. Tools to solve the synthesis problem are readily available, e.g., Hjartarson et al. (2015) which are used in this paper.

2.2 Mixed-sensitivity control architecture

Many requirements on feedback control systems can be directly specified in terms of the induced L_2-norm of weighted sensitivity functions, e.g. disturbance attenuation levels, tracking capabilities, the frequency range of control activity, and robustness. Hence, it is common practice to design induced L_2-norm optimal LPV controllers by mixed-sensitivity loopshaping, see, e.g., Zhou et al. (1996); Skogestad and Postlethwaite (2005). Defining the output sensitivity function $S = (I + G_\rho K_\rho)^{-1}$, the generalized closed loop of the weighted mixed-sensitivity problem shown in Fig. 2 is

$$\begin{bmatrix} z_1 \\ z_2 \end{bmatrix} = \begin{bmatrix} W_e V_e^{-1} & 0 \\ 0 & W_u V_u^{-1} \end{bmatrix} \begin{bmatrix} S & SG_\rho \\ K_\rho S & K_\rho S G_\rho \end{bmatrix} \begin{bmatrix} V_e & 0 \\ 0 & V_d \end{bmatrix} \begin{bmatrix} w_1 \\ w_2 \end{bmatrix}, \tag{6}$$

where W_e and W_u denote frequency dependent weights and V_e, V_u, and V_d constant scaling factors. A high gain in W_e reduces the sensitivity function leading to better tracking and disturbance rejection capabilities. A high gain in W_u reduces the control effort. Hence, W_u can enforce controller roll-off at high frequencies, e.g. to avoid excitation of flexible modes in a system. The static weights are used as the main tuning knobs. Good initial values are obtained based on the maximum expected disturbances (V_d) and the maximum allowable errors (V_e) and inputs (V_u). Theis et al. (2020) present a comprehensive treatment of this parameterisation.

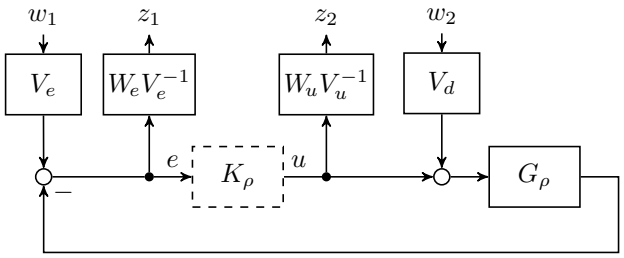

Fig. 2. Weighted four-block mixed-sensitivity problem.

3. SATELLITE ATTITUDE CONTROL

3.1 Satellite and mission

The considered Earth-observation satellite is in an almost circular (eccentricity ≈ 0), sun-synchronous orbit with an altitude of $817km$, an inclination of 99° and an orbital period of ≈ 102 minutes. It orbits in a "normal" mode, with the goal of maintaining its attitude aligned to a chosen reference frame while rejecting external torque disturbances using only reaction wheels. Throughout this paper, plots that detail the dynamical behaviour of the satellite are normalised across frequency, to maintain confidentiality of the model.

The satellite is modelled as a rigid central body with three flexible appendages; two scatterometers and the solar array which completes one full rotation each orbit to maintain its orientation to the sun. The central body is described by the linear Newton-Euler equations (7) with mass m_{CB} and inertia J_{CB}. Given the small angular rates of the problem, non-linearities are neglected.

$$\begin{pmatrix} \Sigma f_{\text{ext}} \\ \Sigma \tau_{\text{ext}} \end{pmatrix} = \begin{bmatrix} m_{\text{CB}} I_{3\times 3} & 0_{3\times 3} \\ 0_{3\times 3} & J_{\text{CB}} \end{bmatrix} \begin{pmatrix} \ddot{r} \\ \dot{\omega} \end{pmatrix} \tag{7}$$

The sum of external forces f_{ext} and torques τ_{ext} acting on the spacecraft result in a translational and rotational acceleration ($\ddot{r}$ and $\dot{\omega}$ respectively). The flexible appendages (FA) are each modelled as a hybrid-cantilever beam connected to the central body at a hinge point P (8). L_P describes the modal contributions of the flexible appendage. Each second-order mode (denoted i) has damping ζ_i and natural frequency ω_i.

$$\begin{aligned} \begin{pmatrix} f^P \\ \tau^P \end{pmatrix} &= \begin{bmatrix} m_{\text{FA}} I_{3\times 3} & 0_{3\times 3} \\ 0_{3\times 3} & J_{\text{FA}} \end{bmatrix} \begin{pmatrix} \ddot{r}_{\text{FA}} \\ \dot{\omega}_{\text{FA}} \end{pmatrix} + L_P^T \ddot{\eta} \\ -L_P \begin{pmatrix} \ddot{r}_{\text{FA}} \\ \dot{\omega}_{\text{FA}} \end{pmatrix} &= \ddot{\eta} + diag(2\zeta_i\omega_i)\dot{\eta} + diag(\omega_i^2)\eta \end{aligned} \tag{8}$$

As the solar array rotates, ζ_i and ω_i change, as does the location of the centre of mass. Thus the overall spacecraft dynamics described by (7) and (8) change as a function of the solar array angular position θ_{SA}. This describes the LPV nature of the plant. Fig. 3 demonstrates how the plant dynamics vary over a grid of solar array angles, $0 \leq \theta_{\text{SA}} < 360°$.

The external torques on the spacecraft are a summation of the solar radiation pressure torque, aerodynamic torque, gravity gradient torque and magnetic field torque which are calculated using a detailed description of the space

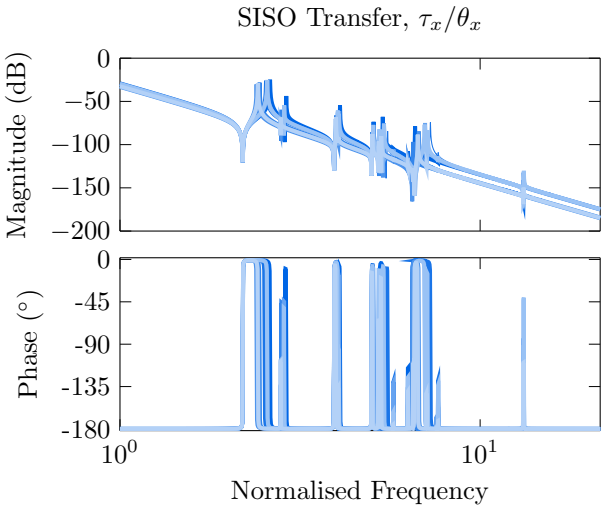

Fig. 3. Satellite dynamics as solar array rotates from minimum angular displacement (——) to maximum (——).

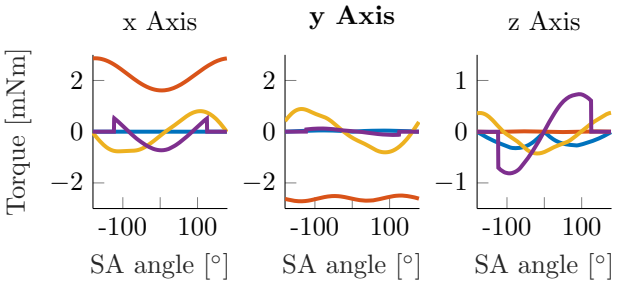

Fig. 4. Aerodynamic (——), gravitational (——), magnetic (——) and solar(——) torques experienced by the satellite during one orbit with respect to the solar array (SA) angle.

environment, for example as in Pisacane (2008). The solar radiation pressure is a summation of momentum exchange for each surface due to the photons colliding with the spacecraft. Similarly, the aerodynamic torque results from collisions with residual atmosphere particles. Both are computed using a geometrical 3-dimensional model of the spacecraft. The gravity gradient torque results from the geo-potential across the spacecraft due to the gravitational field of Earth and the magnetic torque results from the dipole moment created by the magnetic field. Each total torque experienced by the satellite in the body reference frame, as a function of the solar array angle during one orbit, is shown in Fig. 4.

The satellite navigates using star tracker fusion which introduces sensor noise described by high and low spacial frequency error (HSFE, LSFE) and temporal error (TE).The spectral errors are modelled as first-order Gauss-Markov processes and the temporal error can be considered white noise, as is common practice in industry.

3.2 Control problem definition

The satellite and mission describe a multi-input multi-output (MIMO) tracking control problem. The goal is to track a 0 reference attitude described in the spacecraft

Table 1. Pointing metrics (Ott et al., 2011)

Metric	Type	Time domain
APE	absolute (abs)	$\sigma^2_{abs} = E\left[e(t) - \mu_{abs})^2\right]$
RPE	windowed variance (wv)	$\sigma^2_{wv}(\Delta t) = E\left[\left\langle (e(t) - \langle e(t)\rangle_{\Delta t})^2 \right\rangle_{\Delta t}\right]$
PDE	windowed mean stability (wms)	$\sigma^2_{wms}(\Delta t, \Delta t_s) = E\left[\left(\langle e(t)\rangle_{\Delta t} - \langle e\left(t - \Delta t_s\right)\rangle_{\Delta t}\right)^2\right]$

body frame, θ, using only torque input generated by the reaction wheels, τ, also described in the body frame. Sensor noise must be attenuated and external disturbance torques must be rejected such that the closed loop system is able to achieve the specified pointing error requirements. Three types of pointing metrics are considered, absolute performance error (APE), relative performance error (RPE) and performance drift error (PDE). For brevity, the descriptions of these metrics are summarised in Table 1. Certain requirements and limitations are also imposed on the design problem in the frequency domain to ensure sufficient robustness of the system; the gain and phase margins must exceed 6dB and 30° respectively, the peak of each flexible mode must be below −6dB and the modulus margin must be greater than 0.5.

4. CONTROLLER DESIGN

Two controllers were designed, one linear time invariant (LTI) and one LPV controller, such that a reasonable comparison could be drawn. Both design procedures followed the mixed-sensitivity process described in section 2.2, while the LPV design made use of sinusoidal parameter dependent storage functions to capture the periodic nature of the plant. The plant used for design only contained the two flexible modes with the lowest frequencies, as these are most influential on the plant dynamics and the loopshaping problem. The augmented plant for the LTI controller was constructed by weighting the nominal plant ($\theta_{\mathrm{SA}} = 0$) in section 3.1, whereas the augmented plant for the LPV design encompassed a discrete grid of plants, each with a unique solar array angle ($0 \leq \theta_{\mathrm{SA}} < 360°$), into one single LPV plant. This was modelled as a **pss**-object, defined in the LPVTools toolbox (Hjartarson et al., 2015). Other than the nature of the augmented plant, the design process and weighting scheme for each controller was largely the same.

All design weights are diagonal. Firstly W_e^{-1} enforces the shape of the sensitivity function. The crossover frequency was pushed as high as possible to maximise the tracking bandwidth while still ensuring the flexible modes are kept below −6dB. At high frequency the gain of W_e^{-1} is 6dB to guarantee the required modulus margin. The tracking bandwidth of the LTI controller had to be relaxed to maintain robustness to the variations in the dynamics. W_u imposes a roll-off on the controller, thus, at frequencies above the available actuator bandwidth the gain is high. The scaling weights were selected intuitively based on the physical constraints of the system. V_e is the maximum pointing error requirement and V_u the maximum torque available from the actuators. V_d was selected such that

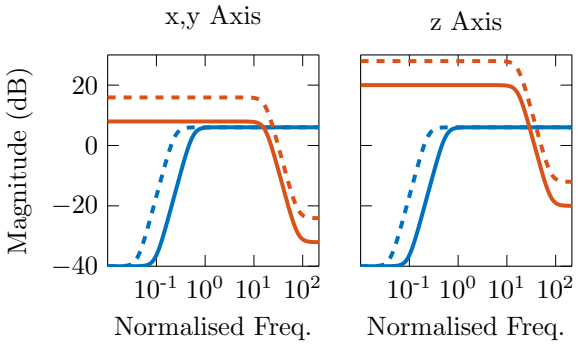

Fig. 5. Imposed requirements on S for K_ρ (——) and K (- - -). Imposed requirements on $K_\rho SG_\rho$ (——) and KSG_ρ (- - -).

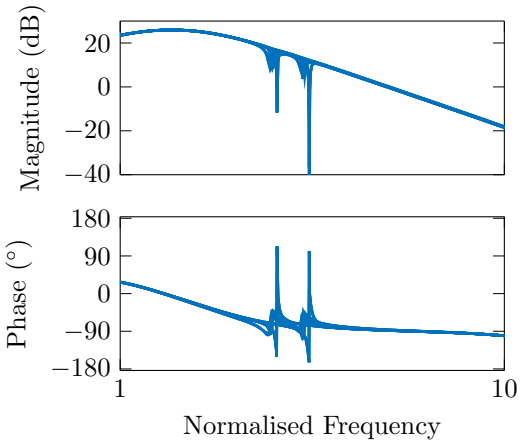

Fig. 6. LPV controller design demonstrates notching of flexible modes.

the ratio of expected disturbance to actuator effort is 20%. For the LTI design the achievable tracking bandwidth was lower in order to maintain the required flexible mode roll off for all plant uncertainties, then the ratio of V_u/V_d was increased to push the controller gain up and speed up the response, see Fig. 5.

The resulting controllers have 18 states and the LPV controller is gridded with the solar array angle at 8 points. The advantage of the LPV design is that it notches the first two flexible modes of the solar array at the corresponding solar array angle, see Fig. 6. This means the LPV controller is less sensitive to the changing frequency of the flexible modes of the solar array as it moves. Thus, while respecting design constraints, the bandwidth of the LPV controller could be pushed higher than that of the LTI controller.

5. CONTROL EVALUATION

The evaluation was completed in the frequency domain using a closed-loop structure, as in Fig. 8, where G_ρ is scheduled with θ_{SA}. To make the evaluation more representative of an industrial-scale project, G_ρ also encompasses uncertainties to cover the lifecycle of the mission, summarised in Table 2. Fig. 7 demonstrates how the dynamics of the spacecraft are affected by the uncertainties. For the frequency domain evaluation, noise and disturbances can

Table 2. Satellite parameter uncertainties.

	Parameter	Range (%)
Central body	Mass	10
	inertia	20
Fuel	Mass	23
	Inertia	scales with mass
Solar array	Mass	10
	Inertia	20
	Cantilever frequency	10
Scatterometers	Mass	10
	Inertia	20
	Cantilever frequency	10

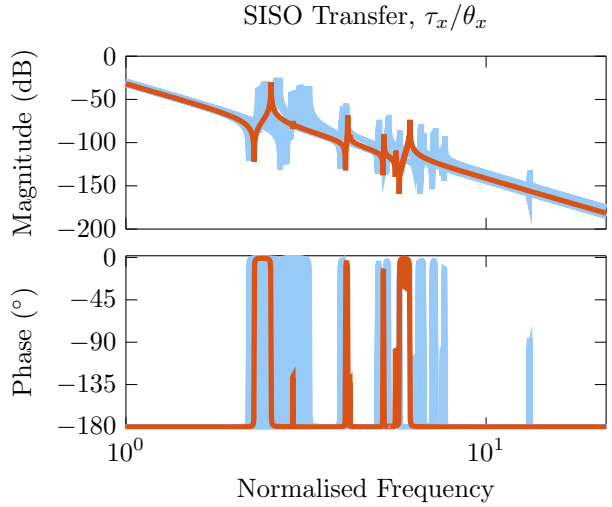

Fig. 7. Nominal plant (—) and a selection of plants over the satellite lifecycle (—).

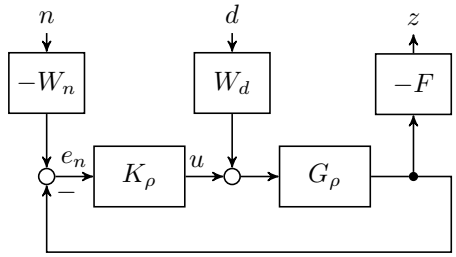

Fig. 8. Block diagram of structure used for analysis.

be approximated as white noise signals passing through filters W_n and W_d respectively. W_n combines the effects of HSFE, LSFE and TE as $W_n = [W_{\text{HSFE}}, W_{\text{LSFE}}, W_{\text{TE}}]$. The spatial error Gauss-Markov processes are equated to first order low pass filters, while the temporal error filter is simply a gain. In comparison, the disturbance filter, W_d, is a rational transfer function approximated from the power spectral density of simulated torque data over the course of three orbits. Similarly, for each error metric in Table 1, a rational transfer function F_i exists that transfers the error signal e into it's respective error metric z_i (Pittelkau and McKinley, 2012). This frequency domain transformation is represented by F in Fig. 8.

In terms of robustness to uncertainties, both controllers meet the requirements with similar distribution. Fig. 9 shows the mean and range of the margins relative to their respective requirements across a grid of plants covering

Table 3. Worst-case achieved pointing error metrics for both K and K_ρ across all uncertainties in the plant (68% confidence level, 1σ).

Metric $\Delta t_1/\Delta t_2/\Delta t_s$ [s]	Req. [μrad]	K $x/y/z$ [μrad]	K_ρ $x/y/z$ [μrad]
APE	300	361/360/639	50.7/49.6/41.9
RPE 6074/-/-	150	334/333/589	49.7/48.6/41.1
RPE 1/-/-	150	0.24/0.23/0.34	0.13/0.11/0.09
PDE 1.07/1.07/0.1	$x = 7$ $y = 3$	0.08/0.08/-	0.04/0.04/-
PDE 0/0/0.1	150	0.08/0.08/0.12	0.04/0.04/0.03

the full range of uncertainties. The LTI design is generally more conservative, although its limiting factor is keeping the flexible mode peaks below −6dB for all uncertainty cases. This is due to its lack of LPV notching behaviour.

The pointing performance was assessed in frequency domain using the principal that the standard deviation σ_e of a signal S_e is equal the H_2-norm of the transfer $H(s)$ from a white noise input to S_e

$$\begin{aligned}\sigma_e &= \left(\tfrac{1}{2\pi}\int_{-\infty}^{\infty} S_e(\omega)d\omega\right)^{0.5} \\ &= \left(\tfrac{1}{2\pi}\int_{-\infty}^{\infty} |H(\omega)|^2 d\omega\right)^{0.5} \\ &= \|H(\omega)\|_2\end{aligned} \tag{9}$$

By assessing the H_2-norm of the transfer function from the input d to the output z as in Fig. 8, the pointing error metrics are obtained (the transfer from noise n was neglected as its effect was negligible). Similarly the 3σ values corresponding to the estimated maximum torque commands were calculated from the H_2-norm of the transfer from d to u. Pointing metric and torque command performance were verified against simulations of a parameter-varying orbit with accurate torque data (as in Fig. 4) and modelled sensor noise. Fig. 10 shows the plotted APE of one simulated orbit. After the initialisation transient, the APE remains within the required bounds, notice there is a second transient when the satellite enters eclipse. Similar results were seen with other performance metrics. All pointing metrics were far exceeded with the LPV design (see Table 3)) while respecting the robustness margins, whereas the LTI design was unable to achieve the APE and RPE pointing requirements. The maximum torque commands for both controller designs were very close, in x and y they are at approximately 60% saturation and in z they are at less than 30% saturation for all plants.

6. CONCLUSION

This paper presented a comprehensive, linear parameter varying (LPV) control design method for the 3-axis attitude tracking of an Earth-observation satellite. The controller is scheduled with the positional angle of a flexible solar array that rotates around the body of the satellite each orbit. The control method demonstrated improved pointing performance when compared to a linear time invariant approach for the same satellite, assessed according to industrial standards. This improvement was due

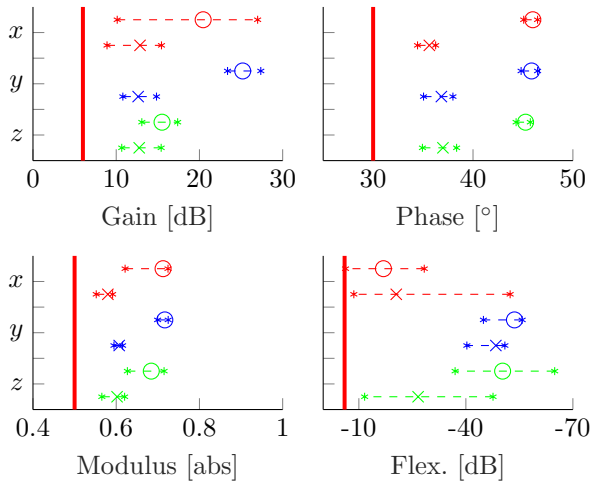

Fig. 9. SISO margin distributions against requirements (—). LTI mean values in x, y and z (○,○ and ○) compared to the LPV mean values (×,× and ×).

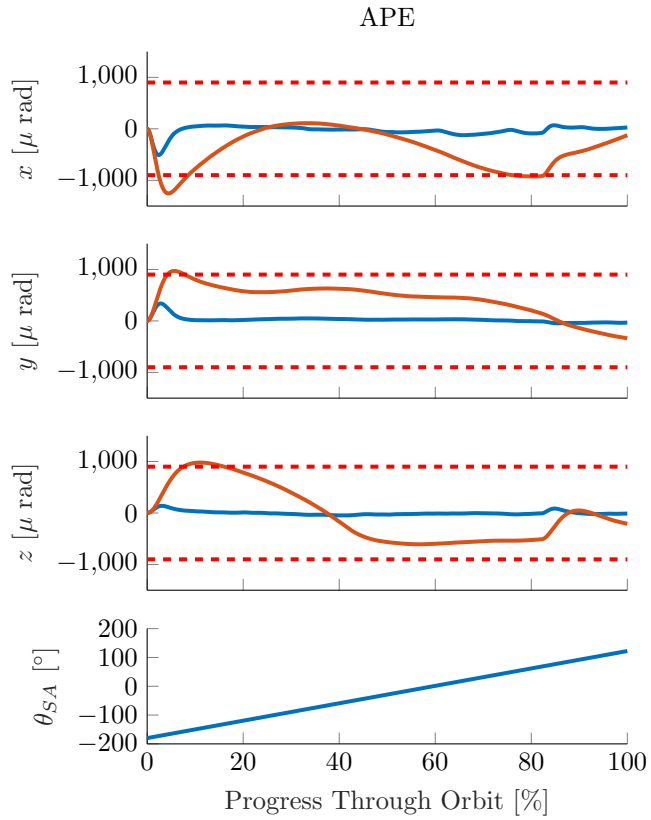

Fig. 10. Pointing performance of LPV (—) and LTI (—) controllers compared to 3σ requirement (- - -).

to the automatic parameter varying notching of the solar array's flexible modes. The presented design process may be developed further for application to automated mode transition during satellite operations by considering modes together as one LPV system.

ACKNOWLEDGEMENTS

The authors gratefully acknowledge the support of Airbus Defense and Space Friedrichshafen for providing the satellite models and giving insights in the industrial process of attitude control design. The authors would like to thank Maurice Martin for the prolonged collaboration on the topic and numerous helpful discussions.

REFERENCES

Alazard, D. and Sanfedino, F. (2020). Satellite dynamics toolbox for preliminary design phase. In *43rd Annual AAS Guidance and Control Conference*, volume 30, 1461–1472.

Angeletti, F., Iannelli, P., Gasbarri, P., Gonzalez, J.P., Ellero, N., Wattrelot, T., Ankersen, F., Sabatini, M., Celani, F., and Palmerini, G. (2022). Robust collocated control of large flexible space structures. *IFAC-PapersOnLine*, 55(25), 85–90.

Biertümpfel, F., Theis, J., and Pfifer, H. (2022). Observer-based synthesis of finite horizon linear time-varying controllers. In *2022 American Control Conference (ACC)*, 2956–2961. IEEE.

ESA (2013). Metop-sg. `https://www.eoportal.org/satellite-missions/metop-sg`.

Guy, N., Alazard, D., Cumer, C., and Charbonnel, C. (2014). Dynamic modeling and analysis of spacecraft with variable tilt of flexible appendages. *Journal of Dynamic Systems, Measurement, and Control*, 136(2), 021020.

Hjartarson, A., Seiler, P., and Packard, A. (2015). LPVTools: A toolbox for modeling, analysis, and synthesis of parameter varying control systems. *IFAC-PapersOnLine*, 48(26), 139–145.

Kassarian, E., Sanfedino, F., Alazard, D., Chevrier, C.A., and Montel, J. (2022). Linear fractional transformation modeling of multibody dynamics around parameter-dependent equilibrium. *IEEE Transactions on Control Systems Technology*.

Ott, T., Benoit, A., Van den Braembussche, P., and Fichter, W. (2011). ESA pointing error engineering handbook. In *8th International ESA Conference on Guidance, Navigation & Control Systems*, 17.

Pisacane, V.L. (2008). *The space environment and its effects on space systems*. American Institute of aeronautics and Astronautics.

Pittelkau, M. and McKinley, W. (2012). Pointing error metrics: displacement, smear, jitter, and smitter with application to image motion mtf. In *AIAA/AAS Astrodynamics Specialist Conference*, 4869.

Skogestad, S. and Postlethwaite, I. (2005). *Multivariable feedback control: analysis and design*. john Wiley & sons.

Theis, J., Ossmann, D., Thielecke, F., and Pfifer, H. (2018). Robust autopilot design for landing a large civil aircraft in crosswind. *Control Engineering Practice*, 76, 54–64.

Theis, J., Pfifer, H., and Seiler, P. (2020). Robust modal damping control for active flutter suppression. *Journal of Guidance, Control, and Dynamics*. Accepted for publication.

Wu, F., Yang, X.H., Packard, A., and Becker, G. (1996). Induced L2-norm control for LPV systems with bounded parameter variation rates. *International Journal of Robust and Nonlinear Control*, 6(9-10), 983–998.

Zhou, K., Doyle, J.C., and Glover, K. (1996). *Robust and Optimal Control*. Prentice Hall, Upper Saddle River, NJ, 1st edition.